

Dynamic nanoscale spatial heterogeneity in a perovskite to brownmillerite topotactic phase transformation

Nicolò D'Anna,^{1,*} Erik S. Lamb,¹ Robin Glefke,¹ Daseul Ham,² Ishmam Nihal,³ Su Yong Lee,² Yayoi Takamura,⁴ and Oleg Shpyrko¹

¹University of California San Diego, La Jolla, CA 92093, USA

²Pohang Light Source-II (PLS-II) Beamline Department,

Pohang Accelerator Laboratory, POSTECH, Pohang 37673, Republic of Korea

³Advanced Light Source, Lawrence Berkeley National Laboratory, Berkeley, California 94720, USA

⁴University of California Davis, Davis, California 95616, USA

Phase transitions are omnipresent in modern condensed matter physics and its applications. In solids, phase transformations typically occur by nucleation and growth under non-equilibrium conditions. Under constant external conditions, *e.g.*, constant heating temperature and pressure, the nucleation and growth dynamics are often thought of as spatially and temporally independent. Here, *in-situ* Bragg X-ray photon correlation spectroscopy (XPCS) reveals nanoscale spatial and dynamical heterogeneity in the perovskite to brownmillerite topotactic phase transformation in $\text{La}_{0.7}\text{Sr}_{0.3}\text{CoO}_3$ (LSCO) thin films under constant reducing conditions over a time-span of multiple hours. Specifically, a timescale associated with domain growth remains stable, with a corresponding domain wall speed of $v_d = 6 \pm 0.5 \times 10^{-4}$ nm/s (2 ± 0.2 nm/h), while a slower timescale, associated with temperature driven de-pinning of domains, leads to accelerating dynamics with timescales following an aging power law with exponent -2.2 ± 0.5 . The experiment demonstrates that Bragg XPCS is a powerful tool to study nanoscale dynamics in phase transformations. The results are relevant for phase engineering of phase-change devices, as they show that nanoscale dynamics, linked to domain and domain-wall motion, can continuously evolve and speed up with time, even hours after the initiation of the phase transformation, with potential repercussions on electrical performance.

1. Introduction

Aging dynamics, commonly observed in glassy materials, are characterized by dynamical relaxation rates varying even under constant external conditions [1–4]. In solids, phase transitions driven by an external stimulus, such as temperature, often results in nucleation and growth of the new phase, forming domains that grow until a new phase-pure state is achieved [5]. In the case of phase transformations where the phases have distinct crystal structures, as is the case for oxygen ion diffusion-driven topotactic phase transformations of metal oxides [6, 7], the nucleation and growth of new domains can be unambiguously detected by Bragg diffraction. In particular, Bragg X-ray photon correlation spectroscopy (XPCS) is a technique particularly well suited to measure slow (>1 s) dynamics linked to nanoscale motion of domains and domain walls in such diffusion-driven phase transformations. It has the potential to reveal whether nanoscale aging dynamics occur under constant external conditions on timescales of several hours. In the current effort to control and utilize phase transitions in phase-change materials for the development of novel technologies [8], understanding spatial and temporal phase transformation heterogeneity becomes highly relevant.

In the scope of novel energy-efficient beyond-semiconductor technologies, there is a broad interest

in taking advantage of tunable phase transformations in functional metal-oxides [8]. Materials where control over the metal-to-insulator transition (MIT) and concomitant structural transition is possible via electric or electrochemical gating are particularly promising [9, 10]. They include cobaltite perovskites [11, 12], vanadium oxides [13–17], Lanthanum Strontium Manganite (LSMO) [18–21], NbO_2 [22, 23], and SmNiO_3 [24–26]. Among such phase-change materials, cobaltite perovskites give access to a particularly rich phase diagram, through a variety of tuning knobs, including epitaxial strain [27, 28] and modification of oxygen ion concentration and distribution [7, 29–32], allowing for manipulation of magnetic and electronic properties [33, 34], leading to many applications such as energy conversion [35], convolutional neural networks, spintronics, and neuromorphic computing [8, 36]. Currently a focus exists on utilizing topotactic phase transformations in perovskite oxides (chemical formula ABO_3), since high oxygen conductivity and low oxygen vacancy formation energy enable phase manipulation through the control of oxygen deficiency δ [32, 37, 38]. Reduction gives access to related phases such as the Grenier ($\text{ABO}_{2.7}$), brownmillerite ($\text{ABO}_{2.5}$), square planar (ABO_2), and Ruddlesden-Popper ($\text{A}_{n+1}\text{B}_n\text{O}_{3n+1}$) phases [39]. In particular, reversible switching from the the perovskite (P) to brownmillerite (BM) phase has been demonstrated in various oxides, including $\text{La}_{0.7}\text{Sr}_{0.3}\text{CoO}_3$ [6], $\text{La}_{0.67}\text{Sr}_{0.33}\text{MnO}_3$ [40], and $\text{YBa}_2\text{Cu}_3\text{O}_{7-\delta}$ [41].

* ndanna@ucsd.edu

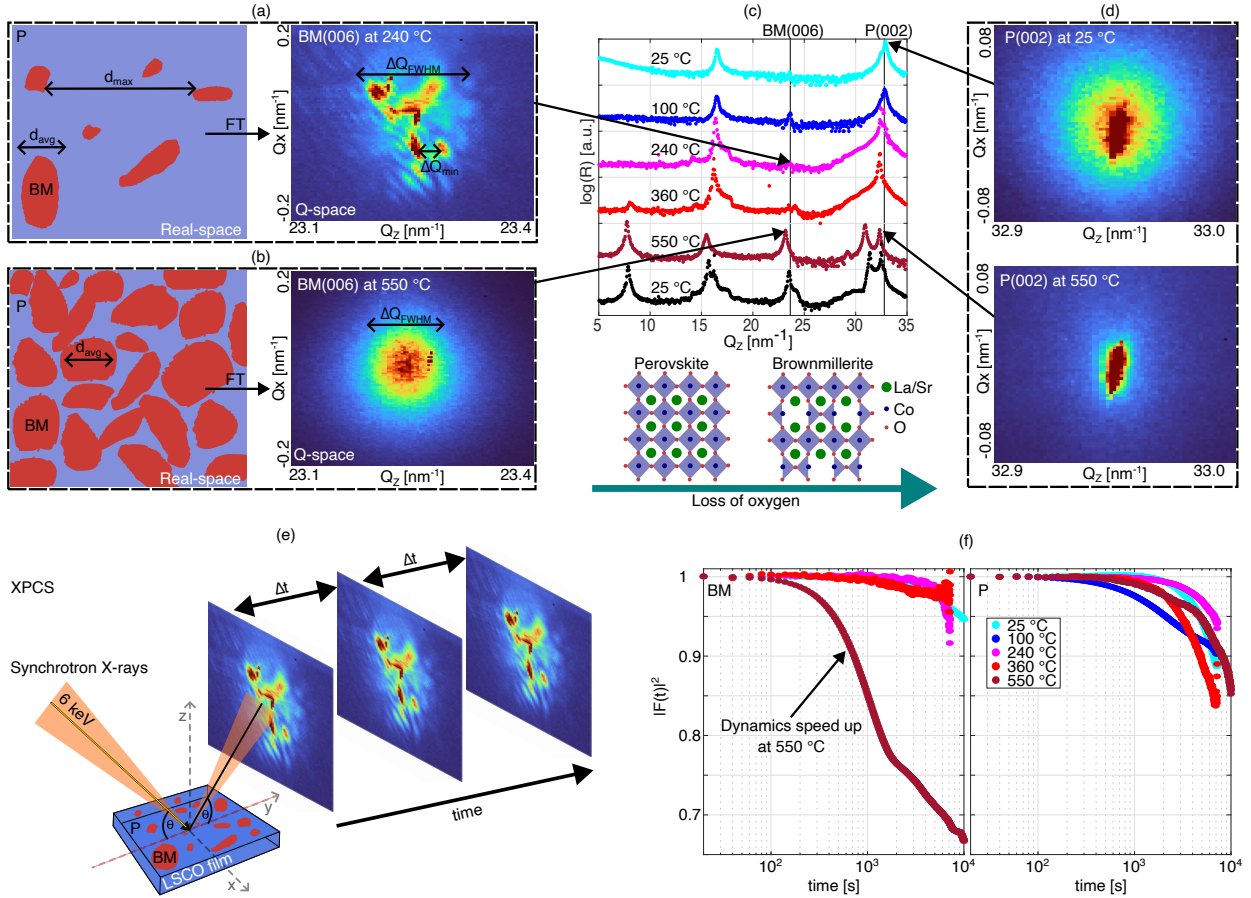


FIG. 1: Coherent x-ray diffraction setup. Brownmillerite BM(006) half-order diffraction Bragg peak (right) observed at 240 °C (a) and 550 °C (b). Illustrations (left) of a dilute (a) and dense (b) BM phase distribution that can lead to such diffraction patterns. The distance ΔQ_{FWHM} in Q-space is inversely proportional to the mean domain size d_{avg} , similarly Q_{min} is inversely proportional to the largest distance between domains within the X-ray beam d_{max} . (c) XRD measurements throughout the experiment, starting at 25 °C (light blue), heating incrementally to 550 °C (dark red), and cooling to 25 °C (black). The crystal structure of the two observed phases is illustrated on the bottom. (d) Perovskite P(002) peak measured at 25 °C and 550 °C. (e) Illustration of the XPCS experiment. (f) Correlation decay of the speckle images measured at all temperatures on the BM(006) peak (left) and the P(002) peak (right), showing a clear increase in dynamics associated with the BM(006) at 550 °C.

Here, Bragg X-ray photon correlation spectroscopy (XPCS) measurements of the perovskite to brownmillerite topotactic phase transformation in $\text{La}_{0.7}\text{Sr}_{0.3}\text{CoO}_3$ (LSCO) thin films resolve the spatial and temporal heterogeneity of the phase transformation. Specifically, it is found that throughout the transformation, timescales linked to the brownmillerite phase continuously evolve as a function of time t_{age} under constant reducing conditions. Results show that prior to the phase transformation, the pristine perovskite phase contains a small amount of preexisting brownmillerite domains ($\approx 0.2\%$), which likely serve as nucleation centers for the phase transformation, in accordance with prior nano-diffraction imaging studies [42]. The results show that under strongly reducing conditions, the brownmillerite domains

are governed by two timescales. The faster timescale, on the order of ~ 1000 s and likely associated with domain growth, is mostly time-independent. The slower timescale, likely associated with domain motion, has a clear time-dependence. In particular, the slow timescales accelerate by almost an order of magnitude over a 9000 s (2.5 h) time-span after setting a constant reducing environment, showing that full equilibrium of phase transformations might take much longer to be achieved than expected from measurements only sensitive to average values for the full volume of the thin film, such as X-ray diffraction (XRD) [43]. Such dynamic heterogeneity, where a fast and slow timescale are observed, are suggested to be a universal feature of glass-forming liquids due to a percolation of mobile and immobile domains [44].

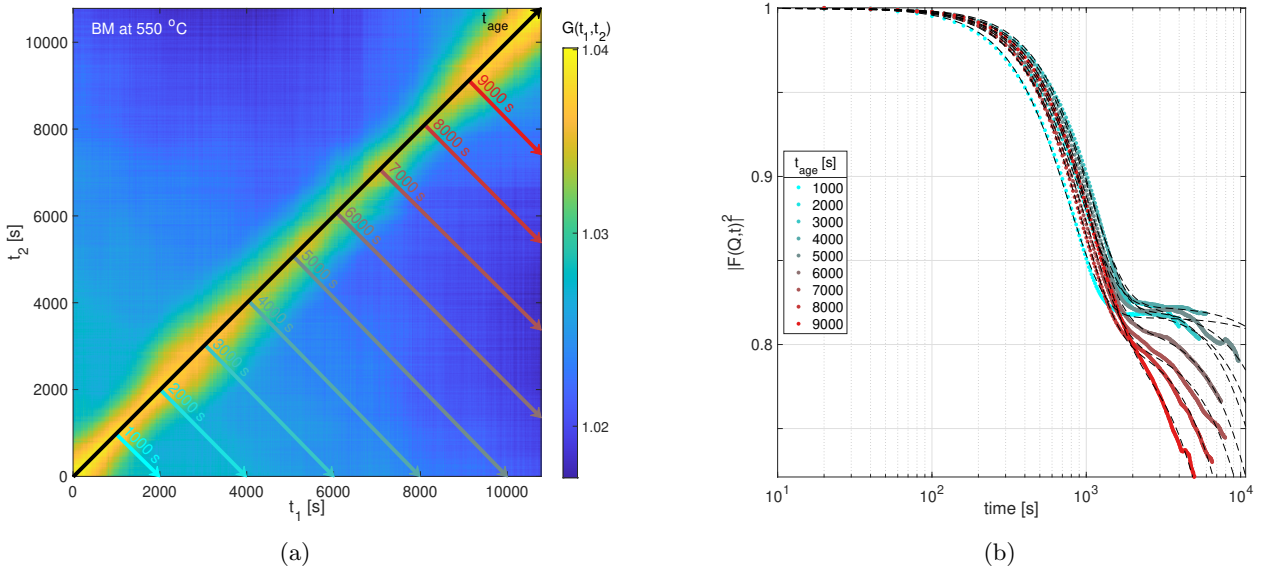


FIG. 2: Dynamic heterogeneity of the phase transformation. (a) Two-time correlation $G(t_1, t_2)$ measured on the brownmillerite (BM) peak at 550 °C. The black arrows indicate the direction of increasing t_{age} and follows $G(t_1, t_2=t_1)$. Perpendicular colored arrows indicate the data used to calculate the one-time correlation functions $g_2^{t_{age}}(t)$ shown in (b). (b) t_{age} dependent correlation decay $|F_{t_{age}}(t)|^2$ obtained from the $g_2^{t_{age}}(t)$ arrows in (a). Dashed lines are fit to the data with the double exponential decay given in Eq. 1.

2. Results

A 20 nm thick LSCO thin layer grown on a $(\text{LaAlO}_3)_{0.3}(\text{Sr}_2\text{AlTaO}_6)_{0.7}$ (LSAT) substrate was studied as a function of annealing temperature in a $P < 1 \times 10^{-3}$ mbar pressure. Temperature was varied from room temperature (25 °C) to 550 °C in five steps. At each temperature, after an alignment X-ray diffraction (XRD) scan, a 2 h long synchrotron XPCS measurement was performed, first on the perovskite P(002) peak, then on the brownmillerite BM(006) half-order peak, followed by another XRD measurement. The X-ray energy was set at 6 keV with a $7 \times 14 \mu\text{m}^2$ focused beam and 3×10^{10} ph/s flux.

XRD results: As confirmed by the XRD measurements, shown in Fig. 1c, the LSCO sample undergoes a phase transformation from the initial perovskite phase to the oxygen deficient brownmillerite phase at $T=550$ °C, as expected in strongly reducing conditions [7]. The high intensity associated with synchrotron X-rays allows the detection of trace amounts of secondary phases which would not be possible with lab-based XRD systems. While the brownmillerite peak is barely visible in the XRD measurements (see Fig. 1c), it is clearly resolved by a 2D detector, with an example shown in Fig. 1a at 240°C. The brownmillerite peak is a half-order peak, it originates from diffraction on the quadrupled unit cell of the brownmillerite phase (as opposed to the perovskite phase). Since the peak probes crystal distances twice the size of the unit cell, it is at half the Q-vector and is more sensitive to longer lengthscales.

The observed speckle patterns in Fig. 1a, b and d are a consequence of the coherent X-rays used for the mea-

surement. Before the phase transformation, the peak is wide and contains a small number of speckles (Fig. 1a, 240 °C), while after the transformation it is narrower and contains too many speckles to be distinguished separately (Fig. 1b, 550 °C). This is because the width of the peak (ΔQ_{FWHM}) is inversely proportional to the average domain size d_{avg} , and the number of speckles is approximately the number of domains in the region illuminated by the X-ray beam [45]. At 240 °C, the mean domain size is $d_{avg} \approx 60 \pm 5$ nm and there are on the order 20 domains in the illuminated region. At 550 °C, the mean domain size is $d_{avg} \approx 55 \pm 5$ nm. In the dilute case, below the transition temperature, the smallest distance ΔQ_{min} between the speckles gives the largest distance d_{max} separating domains within the illuminated region, here ≈ 300 nm [45]. Figure 1a and b illustrate the real space domain distribution that can lead to the observed Bragg peaks. Importantly, below the transition temperature, the ratio of the number of speckles times their mean dimension and the beam spot size gives a measure of the percentage of the sample in the brownmillerite phase, approximately 0.2% at 240 °C.

XPCS results: The XPCS data collected at each temperature are analyzed by computing the usual two-time intensity-intensity correlation function $G(t_1, t_2) = \frac{I(t_1) \cdot I(t_2)}{\langle I^2 \rangle_t}$, where $\langle I^2 \rangle_t$ denotes the average of the squared intensity over the total acquisition period [46]. Thereafter, by taking slices of $G(t_1, t_2)$ with constant time delays $t_2 - t_1 = t$, the one-time correlation functions $g_2(t)$ is obtained. Finally, the intermediate scattering function $|F(t)|$ is calculated with

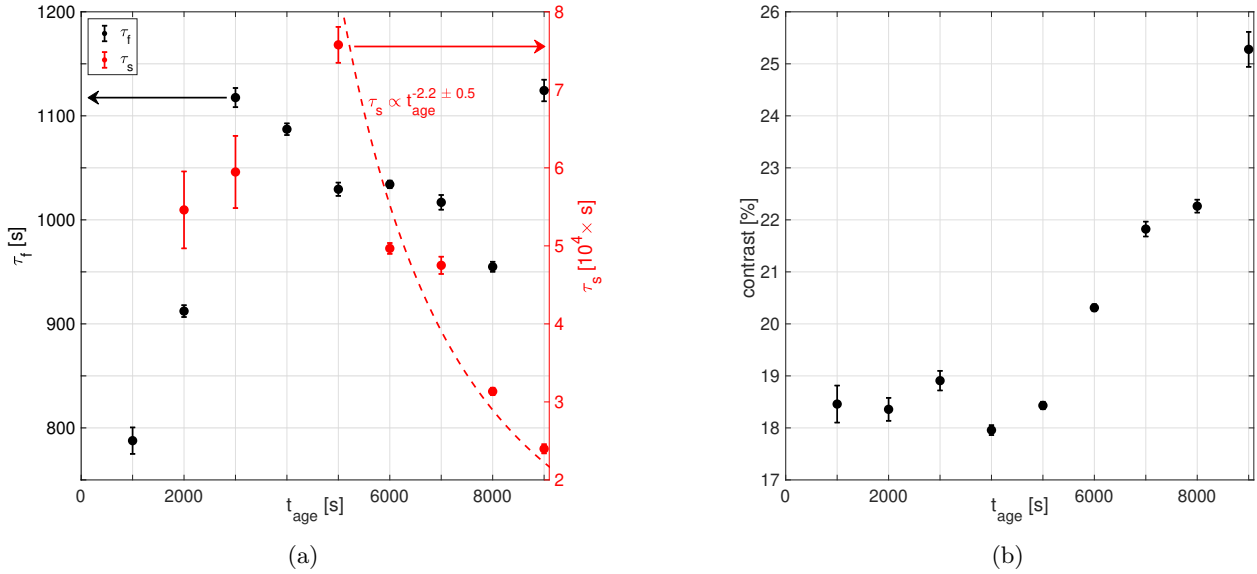


FIG. 3: **Timescales associated with the brownmillerite phase at 550 °C.** (a) Slow and fast timescales, τ_s and τ_f , respectively. τ_s decreases at $t>5000$ s and is fit with a power law (dashed line) with exponent -2.2 ± 0.5 . (b) Contrast as a function of t_{age} , obtained from the second derivative of the fits to Fig. 2b. Increase in contrast indicates that a larger percentage of the diffracting phase is dynamical.

$g_2(t) = 1 + A|F(t)|^2$, where A describes the beam coherence [47]. Figure 1f shows $|F(t)|^2$ obtained on the brownmillerite BM(006) peak (left) and perovskite P(002) peak (right) for all temperatures. At the transition temperature (550 °C), the XPCS data reveals dynamics in the brownmillerite half-order peak with timescales of the order 1000 s, consistent with slow ionic diffusion [48]. Instead, for the perovskite peak and at all other temperatures, the dynamics are considerably slower, as visible in Fig. 1f, and might be dominated by beam and measurement setup instability. Diffraction from a half-order peak is more sensitive to disorder and phase domains, since it originates from reflections on planes separated by twice the lattice constant (smaller Q-vector) and is sensitive to changes on twice the lengthscale, explaining the difference seen between the perovskite and brownmillerite data. Note that the XPCS measurement on the brownmillerite peak is taken at $t>2$ h after setting the sample at 550 °C, such that the transformation is mostly complete (confirmed by stable Bragg peak intensity and width).

The two-time intensity-intensity correlation $G(t_1, t_2)$ obtained from the brownmillerite peak at 550°C is shown in Fig. 2a. The diagonal $t_1 = t_2$ is trivially $G(t_1, t_2) = 1$ and is denoted as the aging time t_{age} (black arrow). Taking cuts perpendicular to $t_1 = t_2$ (colored arrows), correspond to calculating the one-time correlation functions $g_2^{t_{age}}(t)$ and intermediate scattering function $|F_{t_{age}}(t)|^2$ starting at the specific aging time t_{age} . The $|F_{t_{age}}(t)|^2$ corresponding to the colored arrows in Fig. 2a are shown in Fig. 2b, with the dotted lines fits with a double exponential decay function of the form

$$|F_{t_{age}}(t)| = a * \exp(-(t/\tau_f)^\beta) + (1 - a) * \exp(-(t/\tau_s)^\beta), \quad (1)$$

where τ_f and τ_s are the fast and slow characteristic relaxation times, respectively. β is the stretching exponent and $a \leq 1$ a constant.

Noticeable in Fig. 2b is that $|F_{t_{age}}(t)|^2$ saturates at approximately $\sim 82\%$ for $t_{age} \leq 300$ s, while for $t_{age} > 300$ s a second slow decay becomes visible. The first decay ($t < 1000$ s) corresponds to the fast timescale τ_f and the second decay ($t > 1000$ s) to the slow timescale τ_s in Eq. 1. The fitted values for τ_f and τ_s are shown in Fig. 3a as a function of t_{age} , with τ_f and τ_s on the left and right y-axis, respectively. The β and a fitting parameters are found to be t_{age} independent, with $\beta = 1.6 \pm 0.3$ and $a = 0.12 \pm 0.02$. A β value of 1.5 is indicative of jammed/glassy dynamics [46]. The initial fast decay timescale τ_f has a tendency to increase as a function of t_{age} (corresponding to a slow down in dynamics) and is close to $\tau_f \approx 1000$ s. The slow timescale τ_s undergoes a clear decrease (faster dynamics) with t_{age} , decreasing by almost an order of magnitude over the 10000 s measurement time following a power law exponent -2.2 ± 0.5 .

A measure of the percentage of the brownmillerite phase which is dynamic can be quantified by the contrast associated with the fast decay rate τ_f of the BM(006) Bragg peak. It is obtained by minimizing the second derivative of Eq. 1 using the fitting values from Fig. 2b and is plotted in Fig. 3b. The results show an increase in contrast as a function of t_{age} , with a clear increase for $t_{age} > 5000$ s.

3. Discussion

The data presented in Fig. 2 and 3 might be interpreted as XPCS evidence of nucleation and growth of the brownmillerite phase in LSCO under constant reducing conditions ($T = 550^\circ\text{C}$ and $P < 1 \times 10^{-3}$ mbar). The XPCS data are taken at $t > 2$ h after setting the reducing conditions, ensuring that the dynamics are not due to setup thermal instabilities. A clear sign that the observed dynamics are linked to the phase transition is that they are only seen on the brownmillerite (006) half-order Bragg peak at the transition temperature (Fig. 1f).

The age dependent correlation decay in Fig. 2, may qualitatively be explained by a growth and de-pinning process of brownmillerite domains. Initially, only the motion of domain walls (the transition region between brownmillerite and perovskite phase) contributes to the change in the diffraction pattern, leading to the limited 18% contrast value, meaning that only 18% of the brownmillerite phase within the domains is not static. The non-static part may be due to motion of atoms and defects. The slow timescale τ_s , which speeds up with t_{age} following a power law with exponent -2.2 ± 0.5 , might be linked to de-pinning of brownmillerite domains leading to global domain motion and an increase in the decay contrast visible in Fig. 2b and Fig. 3b. The brownmillerite domain size is estimated to be about 55 ± 5 nm. If the domains were considered to be circular, then an outer band containing 18% of the area would be 5 nm thick. This 5 nm region would corresponds to the domain barrier motion (region where the domain grows) and move at an average speed of $v_d = 6 \pm 0.5 \times 10^{-4}$ nm/s, or $v_d = 2 \pm 0.2$ nm/h (see experimental section for more details). However, nano-diffraction imaging of the P-to-B phase transformation in LSCO/Al and LSCO/Gd heterostructures [42, 49], and VO_2 [50] and V_2O_3 [51, 52] metal-oxides, observed domains to grow by elongation of filaments and to be subject to strain at domain boundaries, which affect the domain shape and ratio of domain wall length to domain size. The brownmillerite BM(006) Bragg peak before the phase transition, Fig. 1a, shows that there already is a small density of brownmillerite (0.2%) domains in the perovskite phase (see experimental section for more details). It is reasonable to postulate that during the phase transition, they act as nucleation centers for the further growth of the brownmillerite phase. These initial domains might be pinned to some defect, for example a line defect as observed by nano-diffraction imaging [49], which can become mobile upon heating in vacuum when the overall crystal structure changes.

The observed timescales, τ_f and τ_s , are consistent with recent electrochemical switching experiments on LSCO thin film devices [48], where oxygen ion diffusion was observed to set the timescales for the perovskite to brownmillerite phase transformation. In particular, the experiments on electrochemical transistors found that switching times depend on the square of the LSCO thin film thickness and that there are three timescales linked to the

transformation that are an order of magnitude different from each other. They are the time t_{start} for the first brownmillerite domains to nucleate, the time t_{end} for the phase-pure brownmillerite to be achieved, and the time t_{off} for the source-drain current ON/OFF ratio to reach a value of 5×10^4 . XPCS measurements can be sensitive to all three timescales and is particularly well-suited to detect the two slower processes, related to t_{end} and t_{off} . This is because XPCS measures atomic-scale distribution and dynamics, including motion induced by oxygen diffusion through the phase domains. The t_{end} and t_{off} times indicate slow brownmillerite domain growth (t_{end}) and a slower final rearrangement of the domains (t_{off}), both expected to be visible with XPCS and indicative of timescales expected from oxygen diffusion in LSCO. For a 20 nm thick LSCO thin film, the times were $t_{start} \approx 50$ s, $t_{end} \approx 100$ s, and $t_{off} \approx 1000$ s. For the thermally driven transformation, XPCS yields timescales in the order of 1000s and 10000s of seconds for τ_f and τ_s , respectively, evolving with t_{age} for up 10000 s. These values are comparable with the electrochemical switching times, indicating that the same oxygen diffusion-limited dynamics govern both types of switching. In particular, the slow timescale τ_s linked to domain motion, might be responsible for the difference between t_{end} (phase-pure brownmillerite) and t_{off} (ON/OFF ratio 5×10^4) in devices.

The XPCS results presented here confirm that the perovskite to brownmillerite phase transformation in LSCO is diffusion-limited and that while the initial formation of brownmillerite domains can be relatively fast (< 1 s, not measured here), the time to reach a final stable state can be hours, depending on the reducing conditions. The stretching exponent obtained from fits to eq. 1, $\beta = 1.6 \pm 0.3$, confirm the picture of a jammed/glassy system, where the motion of each domain affects all the others. Such slow time-dependent aging dynamics may limit device speed performance. It is interesting to note that techniques not sensitive to nano-scale heterogeneity dynamics, such as XRD, are not able to detect slow timescales associated with domain motion once the majority phase is achieved, thus positioning XPCS as an ideal technique for the study of phase transformations. While here XPCS is used to characterize the annealing of LSCO thin films in vacuum, it would be well suited to complement electrochemical switching experiments of perovskite oxides transistors in order to associate electrical performance with nanoscale domain dynamics. Additionally, by utilizing free electron laser X-ray radiation, the measurements could access timescales as fast as picoseconds [53].

4. Conclusion

Synchrotron XPCS and XRD measurements were used to study a 20 nm thick LSCO thin film under reducing conditions. Results show that at $T = 550^\circ\text{C}$ and $P < 1 \times 10^{-3}$ mbar, the perovskite to brownmillerite phase transformation has dynamical heterogeneity, characterized by two timescales of the order 1000 s and

10000 s that are time-dependent, *i.e.*, the sample undergoes aging even at times larger than hours, characteristic of glassy materials and possibly posing a limitation to switching speeds. The two timescales are consistent with oxygen ion diffusion leading to continued brownmillerite phase growth and with de-pinning of brownmillerite domains. XRD measurements show that a low density ($\approx 0.2\%$ of the sample) of brownmillerite domains are present within the perovskite phase preceding the phase transformation, which may act as initial nucleation centers for the phase transformation. Altogether, the XPCS results confirm that the phase transformation is oxygen diffusion-limited. In the aim to optimize LSCO-based devices, it will be beneficial to measure XPCS on LSCO transistors under operation, to associate domain growth and motion timescales with electrical performance.

5. Experimental Section

Sample Preparation: Epitaxial 20 nm $\text{La}_{0.7}\text{Sr}_{0.3}\text{CoO}_3$ thin films were grown on (001)-oriented LSAT substrates by pulsed laser deposition using a KrF excimer laser ($\lambda = 248$ nm). The deposition was performed at a substrate temperature of 700 °C using a laser fluence of 0.8 J/cm² and a repetition rate of 1 Hz. The growth was carried out in 0.3 Torr of O₂, followed by post-deposition cooling to room temperature in 300 Torr of O₂ to ensure proper stoichiometry.

X-ray diffraction and photon correlation spectroscopy: The X-ray photon correlation spectroscopy experiments were conducted at the 9C beamline of the Pohang Light Source-II (PLS-II) [54]. The beam was focused with Kb mirrors to a spot size of 8×16 μm² at 6 keV with a transverse coherence length of approximately 1.6 μm in both directions with a 3×10¹⁰ ph/s flux. Diffraction was measured with an EIGER2 X 1M detector, with 1028×1062 pixels and pixel size 75 μm, placed at 861.29 mm from the sample at an angle $2\theta=22.5^\circ$ for the brownmillerite peak and $2\theta=32.8^\circ$ for the perovskite peak. With the same setup, the 2θ angle was swept while recording total diffraction intensity on the detector for the X-ray diffraction measurements.

During the measurement on the brownmillerite Bragg peak at 550 °C, the total intensity on the detector was almost constant with a decreasing trend, while the full-width at half maximum (proportional to mean domain size) was constant.

Brownmillerite domain percentage calculation in the dilute case: For a single domain of radius R_d , the measured speckle radius ΔQ_s is inversely proportional to $R_d = 2\pi/\Delta Q_s$ since the speckle is the Fourier transform of the domain shape. In the case of many diffracting do-

mains within the beam (dense case), no single speckle is resolvable (see Fig. 1b) and the measured Bragg peak's full-width at half-maximum (FWHM) is proportional to the average domain size radius $R_d = 2\pi/\Delta Q_{FWHM}$. At 240 °C $R_d \approx 60 \pm 5$ nm. In the case of a small number of domains (dilute case), the number of visible speckles (on the order of 20, see Fig. 1a) is equal to the number of domains within the beam [45]. The FWHM of the underlying Bragg peak gives a measure of the average domain size, and the smallest inter-speckle distance ΔQ_{int} gives the largest distance between domains. Thus, multiplying the number of domains by the average domain area $A_d = \pi R_d^2$, gives the total area $A_{tot} = n \times A_d$ occupied by the phase responsible for the Bragg peak. Comparing A_{tot} to the X-ray beam size of 8×16 μm² gives a brownmillerite phase percentage of $\approx 0.2\%$.

Domain growth speed approximation: Assuming circular domains, the average domain area is $A_d = \pi R_d^2$ and the moving domain wall area is $A_w = \pi(R_d + R_w)^2 - \pi R_d^2$, where R_w is the distance that the domain wall traveled during the XPCS scan. The observed correlation contrast is the ratio of the static and dynamic parts of the domain, *i.e.*, $contrast = A_w/A_d = (R_w + R_d)^2/R_d^2 - 1$, which decreases with increasing R_d (for a constant R_w). Rearranging the previous expression leads to $R_w = (\sqrt{contrast + 1} - 1)R_d$. Since the domain growth is attributed to the fast time-scale τ_f , and the change in contrast is attributed to domain motion, the initial contrast is taken to calculate domain growth speed ($\approx 18\%$). The FWHM yields $R_d = 2\pi/\Delta Q_{FWHM} \approx 55 \pm 5$ nm. Thus, at 550 °C, the brownmillerite domains grow by $R_w \approx 5$ nm over the 9000 s measurement time (Fig. 3b), and at a speed $v_d = 6 \pm 0.5 \times 10^{-4}$ nm/s, or $v_d = 2 \pm 0.2$ nm/h.

Domain de-pinning rate approximation: Domain de-pinning rate is calculated based on the increase in contrast from 18 % to 25 % over a 9000 s period (Fig. 3b), resulting in 8×10^{-4} % of domains de-pinning per second.

ACKNOWLEDGMENTS

We acknowledge the Pohang Accelerator Laboratory (PAL) for provision of synchrotron radiation facilities and we would like to thank Su Yong Lee and Daseul Ham for assistance and support in using beamline 9C. This research was supported by the Quantum Materials for Energy Efficient Neuromorphic Computing (Q-MEEN-C), an Energy Frontier Research Center funded by the US Department of Energy (DOE), Office of Science, Basic Energy Sciences, under Award DE-SC0019273.

[1] C. A. Angell, “Formation of glasses from liquids and biopolymers,” *Science*, vol. 267, no. 5206, pp. 1924–1935, 1995.

[2] P. G. Debenedetti and F. H. Stillinger, “Supercooled liquids and the glass transition,” *Nature*, vol. 410, no. 6825, pp. 259–267, 2001.

[3] L. Berthier and D. R. Reichman, “Modern computational studies of the glass transition,” *Nature Reviews Physics*,

vol. 5, no. 2, pp. 102–116, 2023.

[4] G. D’Anna and G. Grémaud, “The jamming route to the glass state in weakly perturbed granular media,” *Nature*, vol. 413, no. 6854, pp. 407–409, 2001.

[5] J. Li and F. L. Deepak, “In situ kinetic observations on crystal nucleation and growth,” *Chemical reviews*, vol. 122, no. 23, pp. 16911–16982, 2022.

[6] D. A. Gilbert, A. J. Grutter, P. D. Murray, R. V. Chopdekar, A. M. Kane, A. L. Ionin, M. S. Lee, S. R. Spurgeon, B. J. Kirby, B. B. Maranville, *et al.*, “Ionic tuning of cobaltites at the nanoscale,” *Physical Review Materials*, vol. 2, no. 10, p. 104402, 2018.

[7] I.-T. Chiu, M.-H. Lee, S. Cheng, S. Zhang, L. Heki, Z. Zhang, Y. Mohtashami, P. N. Lapa, M. Feng, P. Shafer, *et al.*, “Cation and anion topotactic transformations in cobaltite thin films leading to ruddlesden-popper phases,” *Physical Review Materials*, vol. 5, no. 6, p. 064416, 2021.

[8] A. Hoffmann, S. Ramanathan, J. Grollier, A. D. Kent, M. J. Rozenberg, I. K. Schuller, O. G. Shpyrko, R. C. Dynes, Y. Fainman, A. Frano, *et al.*, “Quantum materials for energy-efficient neuromorphic computing: Opportunities and challenges,” *APL Materials*, vol. 10, no. 7, 2022.

[9] A. Sawa, “Resistive switching in transition metal oxides,” *Materials today*, vol. 11, no. 6, pp. 28–36, 2008.

[10] Y. Li, Z. Wang, R. Midya, Q. Xia, and J. J. Yang, “Review of memristor devices in neuromorphic computing: materials sciences and device challenges,” *Journal of Physics D: Applied Physics*, vol. 51, no. 50, p. 503002, 2018.

[11] S. Zhang and G. Galli, “Understanding the metal-to-insulator transition in $\text{La}_{1-x}\text{Sr}_x\text{CoO}_{3-\delta}$ and its applications for neuromorphic computing,” *npj Computational Materials*, vol. 6, no. 1, p. 170, 2020.

[12] R. Lengsdorf, M. Ait-Tahar, S. Saxena, M. Ellerby, D. Khomskii, H. Micklitz, T. Lorenz, and M. Abd-Elmeguid, “Pressure-induced insulating state in $(\text{La},\text{Sr})\text{CoO}_3$,” *Physical Review B*, vol. 69, no. 14, p. 140403, 2004.

[13] D. McWhan and J. Remeika, “Metal-insulator transition in $(\text{V}_{1-x}\text{Cr}_x)_2\text{O}_3$,” *Physical Review B*, vol. 2, no. 9, p. 3734, 1970.

[14] A. Zylbersztejn and N. F. Mott, “Metal-insulator transition in vanadium dioxide,” *Physical Review B*, vol. 11, no. 11, p. 4383, 1975.

[15] D. McWhan, A. Menth, J. Remeika, W. Brinkman, and T. Rice, “Metal-insulator transitions in pure and doped V_2O_3 ,” *Physical Review B*, vol. 7, no. 5, p. 1920, 1973.

[16] C. Adda, M.-H. Lee, Y. Kalcheim, P. Salev, R. Rocco, N. M. Vargas, N. Ghazikhanian, C.-P. Li, G. Albright, M. Rozenberg, *et al.*, “Direct observation of the electrically triggered insulator-metal transition in V_3O_5 far below the transition temperature,” *Physical Review X*, vol. 12, no. 1, p. 011025, 2022.

[17] C. W. Rischau, S. Gariglio, J.-M. Triscone, and J. del Valle, “Resistive switching of VO_2 films grown on a thermal insulator,” *Physical Review Applied*, vol. 22, no. 1, p. 014021, 2024.

[18] P. Salev, E. Kisiel, D. Sasaki, B. Gunn, W. He, M. Feng, J. Li, N. Tamura, I. Poudyal, Z. Islam, *et al.*, “Local strain inhomogeneities during electrical triggering of a metal-insulator transition revealed by X-ray microscopy,” *Proceedings of the National Academy of Sciences*, vol. 121, no. 34, p. e2317944121, 2024.

[19] P. Salev, L. Fratino, D. Sasaki, R. Berkoun, J. Del Valle, Y. Kalcheim, Y. Takamura, M. Rozenberg, and I. K. Schuller, “Transverse barrier formation by electrical triggering of a metal-to-insulator transition,” *Nature communications*, vol. 12, no. 1, p. 5499, 2021.

[20] T.-Y. Chen, D. Y. Sasaki, B. Achinuq, N. Ghazikhanian, P. Salev, H. Ohldag, A. Scholl, I. K. Schuller, Y. Takamura, and A. D. Kent, “Voltage-induced magnetic domain evolution in a phase-change material,” *Applied Physics Letters*, vol. 125, no. 26, 2024.

[21] T.-Y. Chen, H. Ren, N. Ghazikhanian, R. E. Hage, D. Y. Sasaki, P. Salev, Y. Takamura, I. K. Schuller, and A. D. Kent, “Electrical control of magnetic resonance in phase change materials,” *Nano Letters*, vol. 24, no. 37, pp. 11476–11481, 2024.

[22] M. D. Pickett, G. Medeiros-Ribeiro, and R. S. Williams, “A scalable neuristor built with mott memristors,” *Nature materials*, vol. 12, no. 2, pp. 114–117, 2013.

[23] L. Gao, P.-Y. Chen, and S. Yu, “NbOx based oscillation neuron for neuromorphic computing,” *Applied physics letters*, vol. 111, no. 10, 2017.

[24] J. Shi, S. D. Ha, Y. Zhou, F. Schoofs, and S. Ramanathan, “A correlated nickelate synaptic transistor,” *Nature communications*, vol. 4, no. 1, p. 2676, 2013.

[25] S. D. Ha, U. Vetter, J. Shi, and S. Ramanathan, “Electrostatic gating of metallic and insulating phases in SmNiO_3 ultrathin films,” *Applied Physics Letters*, vol. 102, no. 18, 2013.

[26] C. W. Rischau, P. Torruella, C.-Y. Hsu, S. Gariglio, D. T. Alexander, J.-M. Triscone, and J. del Valle, “Synaptic and neuronal functionalities on a single oxide film via interface engineering,” *Physical Review Applied*, vol. 23, no. 2, p. 024051, 2025.

[27] M. Feng, N. J. Ahlm, A. M. Kane, I. Chiu, D. Y. Sasaki, P. Shafer, A. Mehta, Y. Takamura, *et al.*, “Strain-and thickness-dependent magnetic properties of epitaxial $\text{la}_0.67\text{sr}_0.33\text{coo}_3/\text{la}_0.67\text{sr}_0.33\text{mno}_3$ bilayers,” *Journal of Applied Physics*, vol. 132, no. 19, 2022.

[28] D. Shin, S. Yoon, S. Song, S. Park, H. N. Lee, and W. S. Choi, “Tunable ferromagnetism in lacoo_3 epitaxial thin films,” *Advanced Materials Interfaces*, vol. 9, no. 20, p. 2200433, 2022.

[29] R. Caciuffo, D. Rinaldi, G. Barucca, J. Mira, J. Rivas, M. Senaris-Rodriguez, P. Radaelli, D. Fiorani, and J. B. Goodenough, “Structural details and magnetic order of $\text{la}_{1-x}\text{sr}_x\text{coo}_3$ ($x < \sim 0.3$),” *Physical Review B*, vol. 59, no. 2, p. 1068, 1999.

[30] J. Wu and C. Leighton, “Glassy ferromagnetism and magnetic phase separation in $\text{la}_{1-x}\text{sr}_x\text{coo}_3$,” *Physical Review B*, vol. 67, no. 17, p. 174408, 2003.

[31] D. A. Gilbert, J. Olamit, R. K. Dumas, B. J. Kirby, A. J. Grutter, B. B. Maranville, E. Arenholz, J. A. Borchers, and K. Liu, “Controllable positive exchange bias via redox-driven oxygen migration,” *Nature communications*, vol. 7, no. 1, p. 11050, 2016.

[32] H. Jeen, W. S. Choi, J. W. Freeland, H. Ohta, C. U. Jung, and H. N. Lee, “Topotactic phase transformation of the brownmillerite $\text{srcoo}_2.5$ to the perovskite $\text{srcoo}_3-\delta$,” *arXiv preprint arXiv:1307.3932*, 2013.

[33] M. Feng, J. Li, S. Zhang, A. Pofelski, R. E. Hage, C. Klewe, A. T. N’diaye, P. Shafer, Y. Zhu, G. Galli, *et al.*, “Hydrogen-induced topotactic phase transformations of cobaltite thin films,” *The Journal of Physical*

Chemistry C, vol. 128, no. 40, pp. 17124–17133, 2024.

[34] V. Chaturvedi, W. M. Postiglione, R. D. Chakraborty, B. Yu, W. Tabiš, S. Hameed, N. Biniskos, A. Jacobson, Z. Zhang, H. Zhou, *et al.*, “Doping-and strain-dependent electrolyte-gate-induced perovskite to brownmillerite transformation in epitaxial $la_{1-x} sr_x coo_3-\delta$ films,” *ACS applied materials & interfaces*, vol. 13, no. 43, pp. 51205–51217, 2021.

[35] N. Lu, Z. Zhang, Y. Wang, H.-B. Li, S. Qiao, B. Zhao, Q. He, S. Lu, C. Li, Y. Wu, *et al.*, “Enhanced low-temperature proton conductivity in hydrogen-intercalated brownmillerite oxide,” *Nature Energy*, vol. 7, no. 12, pp. 1208–1216, 2022.

[36] G. Chen, M. Robertson, M. Hoffmann, C. Ophus, A. L. Fernandes Cauduro, R. Lo Conte, H. Ding, R. Wiesendanger, S. Blügel, A. K. Schmid, *et al.*, “Observation of hydrogen-induced dzyaloshinskii-moriya interaction and reversible switching of magnetic chirality,” *Physical Review X*, vol. 11, no. 2, p. 021015, 2021.

[37] H. Jeen, W. S. Choi, M. D. Biegalski, C. M. Folkman, I.-C. Tung, D. D. Fong, J. W. Freeland, D. Shin, H. Ohta, M. F. Chisholm, *et al.*, “Reversible redox reactions in an epitaxially stabilized $srco_3$ x oxygen sponge,” *Nature materials*, vol. 12, no. 11, pp. 1057–1063, 2013.

[38] J. Walter, H. Wang, B. Luo, C. D. Frisbie, and C. Leighton, “Electrostatic versus electrochemical doping and control of ferromagnetism in ion-gel-gated ultrathin $la_{0.5}sr_{0.5}co_3-\delta$,” *ACS nano*, vol. 10, no. 8, pp. 7799–7810, 2016.

[39] M. T. Anderson, J. T. Vaughney, and K. R. Poepelmeier, “Structural similarities among oxygen-deficient perovskites,” *Chemistry of materials*, vol. 5, no. 2, pp. 151–165, 1993.

[40] A. J. Grutter, D. A. Gilbert, U. Alaan, E. Arenholz, B. B. Maranville, J. A. Borchers, Y. Suzuki, K. Liu, and B. J. Kirby, “Reversible control of magnetism in $la_{0.67}sr_{0.33}mn_3$ through chemically-induced oxygen migration,” *Applied Physics Letters*, vol. 108, no. 8, 2016.

[41] P. D. Murray, D. A. Gilbert, A. J. Grutter, B. J. Kirby, D. Hernandez-Maldonado, M. Varela, Z. E. Brubaker, W. Liyanage, R. V. Chopdekar, V. Taufour, *et al.*, “Interfacial-redox-induced tuning of superconductivity in $yba_2cu_3o_7-\delta$,” *ACS Applied Materials & Interfaces*, vol. 12, no. 4, pp. 4741–4748, 2019.

[42] S. Smith, J. Mehta, M. Madhavi, C. Li, S. Jeppson, J. Li, M. Feng, M. Holt, T. Zhou, Z. Cai, *et al.*, “Nanodiffraction imaging of ionically driven phase separation in cobaltite heterostructures,” *APL Materials*, vol. 13, no. 7, 2025.

[43] H. M. Rietveld, “A profile refinement method for nuclear and magnetic structures,” *Applied Crystallography*, vol. 2, no. 2, pp. 65–71, 1969.

[44] L. Gao, H.-B. Yu, T. B. Schröder, and J. C. Dyre, “Unified percolation scenario for the α and β processes in simple glass formers,” *Nature Physics*, pp. 1–9, 2025.

[45] M. Bluschke, R. Basak, A. Barbour, A. N. Warner, K. Fürsich, S. Wilkins, S. Roy, J. Lee, G. Christiani, G. Logvenov, *et al.*, “Imaging mesoscopic antiferromagnetic spin textures in the dilute limit from single-geometry resonant coherent x-ray diffraction,” *Science Advances*, vol. 8, no. 29, 2022.

[46] O. G. Shpyrko, “X-ray photon correlation spectroscopy,” *Synchrotron Radiation*, vol. 21, no. 5, pp. 1057–1064, 2014.

[47] M. Sutton, S. Mochrie, T. Greytak, S. Nagler, L. Berman, G. Held, and G. Stephenson, “Observation of speckle by diffraction with coherent x-rays,” *Nature*, vol. 352, no. 6336, pp. 608–610, 1991.

[48] J. Liang, W. M. Postiglione, M. Van Someren, N. Nandakumaran, B. W. Jeong, C. D. Frisbie, and C. Leighton, “Limits on topotactic transformation speed in electrolyte-gate $la_{0.5}sr_{0.5}co_3-\delta$ electrochemical transistors,” *ACS nano*, 2025.

[49] G. Rippy, L. Trinh, A. M. Kane, A. L. Ionin, M. S. Lee, R. V. Chopdekar, J. M. Christiansen-Salameh, D. A. Gilbert, A. J. Grutter, P. D. Murray, *et al.*, “X-ray nanodiffraction studies of ionically controlled nanoscale phase separation in cobaltites,” *Physical Review Materials*, vol. 3, no. 8, p. 082001, 2019.

[50] A. G. Shabalin, J. Del Valle, N. Hua, M. J. Cherukara, M. V. Holt, I. K. Schuller, and O. G. Shpyrko, “Nanoscale imaging and control of volatile and non-volatile resistive switching in VO_2 ,” *Small*, vol. 16, no. 50, p. 2005439, 2020.

[51] N. D’Anna, N. Ghazikhanian, E. S. Lamb, E. Zatterin, M. Wan, A. Thorshov, I. K. Schuller, and O. Shpyrko, “Self-strain suppression of the metal-to-insulator transition in phase-change oxide devices,” *Small*, p. e09287, 2025.

[52] Z. Shao, A. Luo, E. Barazani, T. Zhou, Z. Cai, M. V. Holt, Y. Kalcheim, and A. Singer, “X-ray nanoimaging of a heterogeneous structural phase transition in V_2O_3 ,” *Nano Letters*, 2025.

[53] X. Yu, L. Wu, Y. Lin, J. Diao, J. Liu, J. Hallmann, U. Boesenberg, W. Lu, J. Möller, M. Scholz, *et al.*, “Ultrafast bragg coherent diffraction imaging of epitaxial thin films using deep complex-valued neural networks,” *npj Computational Materials*, vol. 10, no. 1, p. 24, 2024.

[54] D. Ham, D. Nam, C. Song, and S. Y. Lee, “Upgrade of the coherent x-ray scattering beamline at pohang light source ii,” *Synchrotron Radiation*, vol. 33, no. 1, 2026.